ChemPubSoc Europe

DOI: 10.1002/chem.201504117

CHEMISTRY
A European Journal
Full Paper

Polar Materials

$K_2Au(IO_3)_5$ and β-$KAu(IO_3)_4$: Polar Materials with Strong SHG Responses Originating from Synergistic Effect of AuO_4 and IO_3 Units**

Xiang Xu,[a] Chun-Li Hu,[a] Bing-Xuan Li,[b] and Jiang-Gao Mao*[a]

Abstract: Two new polar potassium gold iodates, namely, $K_2Au(IO_3)_5$ (*Cmc*2_1) and β-$KAu(IO_3)_4$ (*C*2), have been synthesized and structurally characterized. Both compounds feature zero-dimensional polar $[Au(IO_3)_4]^-$ units composed of an AuO_4 square-planar unit coordinated by four IO_3^- ions in a monodentate fashion. In β-$KAu(IO_3)_4$, isolated $[Au(IO_3)_4]^-$ ions are separated by K^+ ions, whereas in $K_2Au(IO_3)_5$, isolated $[Au(IO_3)_4]^-$ ions and non-coordinated IO_3^- units are separated by K^+ ions. Both compounds are thermally stable up to 400 °C and exhibit high transmittance in the NIR region ($\lambda =$ 800–2500 nm) with measured optical band gaps of 2.65 eV for $K_2Au(IO_3)_5$ and 2.75 eV for β-$KAu(IO_3)_4$. Powder second-harmonic generation measurements by using $\lambda = 2.05$ μm laser radiation indicate that $K_2Au(IO_3)_5$ and β-$KAu(IO_3)_4$ are both phase-matchable materials with strong SHG responses of approximately 1.0 and 1.3 times that of $KTiOPO_4$, respectively. Theoretical calculations based on DFT methods confirm that such strong SHG responses originate from a synergistic effect of the AuO_4 and IO_3 units.

Introduction

Metal iodates are an important family of functional materials, especially as second-order nonlinear optical (NLO) crystals.[1–6] Famous examples are α-$LiIO_3$ and α-HIO_3, which are excellent piezoelectric crystals as well as NLO crystals.[7,8] In metal iodates, I^{5+} ions usually exhibit the trigonal-pyramidal coordination geometry of IO_3^-. Such a polar and asymmetric IO_3^- structure unit is favorable for the formation of non-centrosymmetric (NCS) structures, which is a precondition of second-harmonic generation (SHG) properties. Furthermore, due to the presence of stereo-active lone pair electrons on the central I^{5+} ions, IO_3^- possesses large microscopic second-order NLO susceptibilities, which imply that IO_3^- is a charming NLO-active anionic group. According to the anionic group theory proposed by Chen et al., the overall second harmonic generation coefficient of a NLO crystal should be mainly attributed to the geometrical superposition of the microscopic second-order susceptibility tensors of NLO-active anionic groups.[9] Hence, increasing the density and adjusting the packing fashion of IO_3^- units in a structure should be an effective approach to improve its NLO performance. Recently, it has been reported that polymerization of discrete IO_3^- groups into polyiodate units can form new types of structures with relatively higher densities of NLO-active IO_3^- units.[10–14] For example, NaI_3O_8,[12] α-AgI_3O_8, and β-AgI_3O_8[14] all containing trinuclear $I_3O_8^-$ ions exhibit strong SHG responses of about 18.7, 9.0, and 8.0 times, respectively, that of KH_2PO_4 (KDP). Another effective route for designing new NLO metal iodates is the incorporation of a second cation into the ternary metal iodates, which affords abundant new structures.[15–21] Mostly, transition-metal ions with d^0 electronic configurations (i.e., Ti^{4+}, Nb^{5+}, V^{5+}, Mo^{6+}, etc.) are introduced into iodates because they usually form distorted MO_6 (M represent the d^0 transition metal) octahedra, which are also polar and SHG active.[22] By using such a strategy, a large number of mixed metal iodates with excellent SHG properties has been discovered, such as $Li_2Ti(IO_3)_6$,[16a] $BaNbO(IO_3)_5$,[18a] and $NaVO_2(IO_3)_2(H_2O)$.[18c]

Different from d^0 transition-metal ions, noble-metal ions with d^8 electronic configurations (e.g., Au^{3+} or Pd^{2+}) tend to form a square-planar MO_4 ($M = Au^{3+}$ or Pd^{2+}) coordination geometry. From the perspective of the structural design for NLO property, the introduction of such MO_4 units into iodates is expected to form different connection fashions of MO_4 and IO_3 units and may further afford various iodates with favorable arrangement of NLO-active IO_3 units. However, explorations of iodates containing d^8 noble-metal ions (e.g., Au^{3+} or Pd^{2+}) are still limited.[23,24] Within these reported iodates, the square-planar MO_4 ($M = Au^{3+}$ or Pd^{2+}) unit shares corners with four IO_3 units to form a new type of anionic group of the formula

[a] *Dr. X. Xu, Dr. C.-L. Hu, Prof. Dr. J.-G. Mao*
State Key Laboratory of Structural Chemistry
Fujian Institute of Research on the Structure of Matter
Chinese Academy of Sciences, Fuzhou, 350002 (P.R. China)
Fax: (+86) 591-6317-3121
E-mail: mjg@fjirsm.ac.cn

[b] *B.-X. Li*
Key Laboratory of Optoelectronic Materials Chemistry and Physics
Fujian Institute of Research on the Structure of Matter
Chinese Academy of Sciences, Fuzhou, 350002 (P.R. China)

[**] *SHG = second-harmonic generation.*

Supporting information for this article (containing bond lengths and angles, powder XRD patterns, IR spectra, calculated dipole moments, band structures, and molecular orbitals for the title compounds) is available on the WWW under http://dx.doi.org/10.1002/chem.201504117.

$[M(IO_3)_4]^{n-}$ with a polar or non-polar configuration. In the non-polar $[M(IO_3)_4]^{n-}$ structure, the four IO_3 units are located at both sides of the MO_4 plane and are related through inversion centers, and in the polar $[M(IO_3)_4]^{n-}$ structure, the four IO_3 units sit on the same side of the MO_4 plane. When the polar $[M(IO_3)_4]^{n-}$ groups are aligned, they produce strong SHG responses, for example, $RbAu(IO_3)_4$[24b] exhibits a SHG response of 1.33 times that of $KTiOPO_4$ (KTP). As for the monovalent metal gold(III) iodate systems, our group has reported six compounds with the same formula of $AAu(IO_3)_4$ (A = Na, Rb, Cs, and Ag), among which the Na and Cs compounds each displays two different types of structures.[24b] However, for K-containing gold iodates, there is only one compound, namely $KAu(IO_3)_4$, reported by the group of Albrecht-Schmitt in 2007.[23] Despite it crystallizes in the polar space group *P*1, its SHG property has not been studied. To further explore the effect of the counter cations and of the synthetic conditions on the structures and properties of quaternary gold iodates, we have performed the systematic exploration in the K-Au-I-O system. Our research efforts have led to the discoveries of two new polar potassium gold(III) iodates, namely, $K_2Au(IO_3)_5$ (**1**, $Cmc2_1$) and β-$KAu(IO_3)_4$ (**2**, C_2). Herein, we report their syntheses, crystal structures, thermal stabilities, and nonlinear optical properties. Furthermore, theoretical calculations based on DFT method have been performed to understand the origin of the SHG property.

Results and Discussion

By using the same starting materials with different molar ratios, two new polar potassium gold(III) iodates have been synthesized hydrothermally, namely, $K_2Au(IO_3)_5$ (**1**, $Cmc2_1$) and β-$KAu(IO_3)_4$ (**2**, *C*2). Compound **2** features similar zero-dimensional $[Au(IO_3)_4]^-$ ions as those in α-$KAu(IO_3)_4$ (*P*1) reported by Albrecht-Schmitt et al.,[23] but the local symmetry of the $[Au(IO_3)_4]^-$ ions of these two isomers are different. In compound **1**, additional "isolated" $I(1)O_3^-$ ions exist in the lattice. Both compounds **1** and **2** exhibit strong SHG responses and high transmittance in the spectral region of $\lambda = 800$-2500 nm, which is indicative for their potential application as new near-infrared NLO crystals (Table 1).

Table 1. Crystallographic data for $K_2Au(IO_3)_5$ and β-$KAu(IO_3)_4$.

	$K_2Au(IO_3)_5$	β-$KAu(IO_3)_4$
Fw	1149.67	935.67
T [K]	295.2(3)	296.0(1)
crystal system	orthorhombic	monoclinic
space group	$Cmc2_1$	*C*2
a [Å]	11.5949(8)	13.4056(10)
b [Å]	11.6905(6)	5.4229(3)
c [Å]	11.4716(6)	8.3771(5)
β [°]	90	109.184(7)
V [Å^3]	1554.97(15)	575.17(6)
Z	4	2
ρ_{calcd} [g cm^{-3}]	4.911	5.403
μ ($Mo_{K\alpha}$) [mm^{-1}]	19.997	23.944
R_{int}	0.0494	0.0644
GoF on F^2	1.048	0.899
Flack factor	−0.009(14)	−0.033(6)
*R*1, *wR*2 [$I > 2\sigma(I)$][a]	0.0385, 0.0959	0.0240, 0.0448
*R*1, *wR*2 (all data)	0.0396, 0.0983	0.0251, 0.0458

[a] $R_1 = \Sigma||F_c| - |F_o||/\Sigma|F_o|$; $wR_2 = \{\Sigma w[(F_o)^2 - (F_c)^2]^2/\Sigma w[(F_o)^2]^2\}^{1/2}$.

Syntheses

Through hydrothermal reactions of the same starting materials KIO_3, $Au(OH)_3$, and I_2O_5, compounds **1** and **2** as well as the known α-$KAu(IO_3)_4$ can be synthesized. As described in the Experimental Section, single-phases of compounds **1** or **2** can be isolated through adjusting the molar ratios of the raw materials. Compared with compound **2**, compound **1** is more sensitive to the synthetic conditions and required a smaller amount of $Au(OH)_3$ but a larger amount of I_2O_5. The reported α-$KAu(IO_3)_4$ may by present in the product randomly in a very low yield along with a larger amount of compound **2**, but a single phase of α-$KAu(IO_3)_4$ has not been isolated by now on the basis of our experiments. For the preparations of the pure phases of both compounds **1** and **2**, a large excess of KIO_3 is necessary. It was found that colorless $K(IO_3)(HIO_3)$ crystals were easily grown when the reaction products were cooled to room temperature. Hence, the hot reaction products were filtered quickly.

As shown in Figures 1a and b, crystals of compounds **1** and **2** exhibit a similar color (i.e., yellow) but obviously different morphologies. Crystals of compound **1** are prism-shaped and

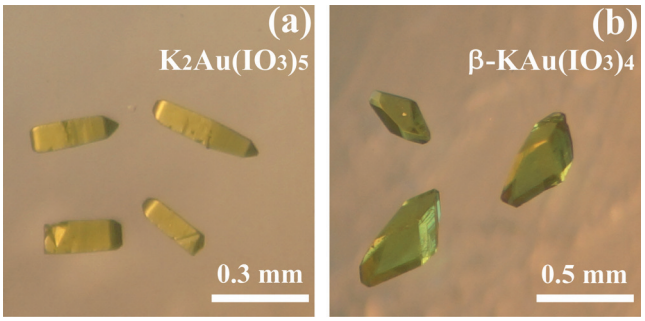

Figure 1. As-grown crystals of a) $K_2Au(IO_3)_5$ and b) β-$KAu(IO_3)_4$.

crystals of compound **2** are granular, which can help us to distinguish them easily. EDS elemental analyses on single crystals give K/Au/I molar ratios of 1.9:1:4.6 for compound **1** and 0.9:1:3.6 for compound **2**, which are in agreement with the molecular formulas of both compounds (Figure S1 in the Supporting Information).

The single-phase nature of the obtained crystals of compounds **1** and **2** were confirmed by the excellent matching of the experimental and simulated powder XRD patterns (Figure S2 in the Supporting Information). Furthermore, Rietveld refinements for the powder XRD patterns were performed by using the program GSAS based on the crystal structure model determined by the single-crystal XRD.[25] As shown in Figure 2, the calculated XRD patterns of the Rietveld refinements fit well

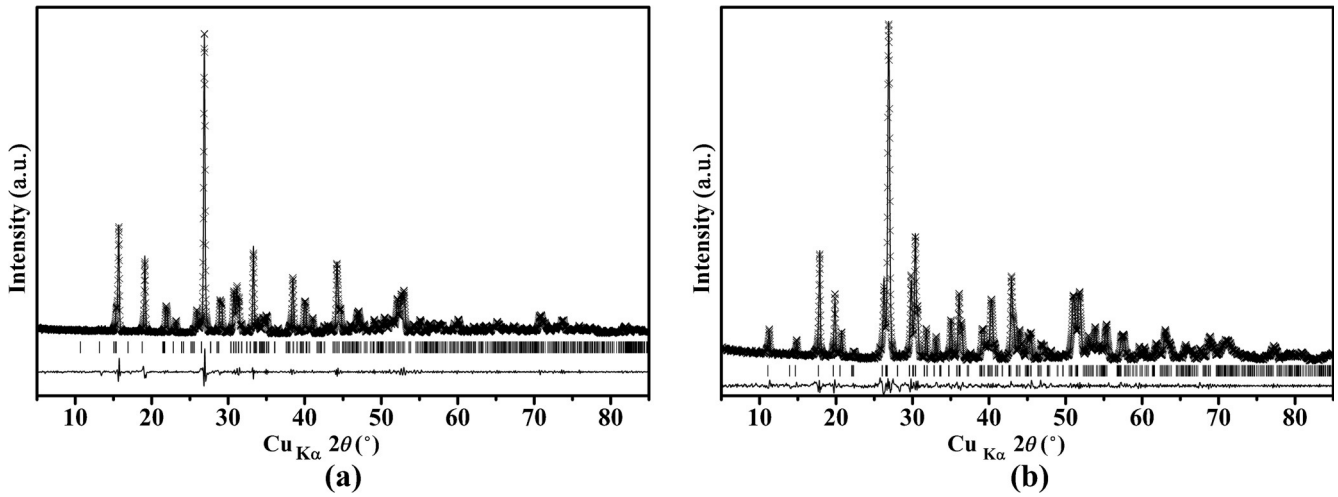

Figure 2. Rietveld refinement plots of the powder XRD patterns for a) $K_2Au(IO_3)_5$ and b) β-$KAu(IO_3)_4$: experimental data (cross), calculated data (solid line), peak positions (tick marks), and difference curves (bottom solid line).

with the observed patterns. The refined lattice parameters (a = 11.5837(14), b = 11.7288(15), and c = 11.4808(14) Å for compound **1**, and a = 13.4255(4), b = 5.4301(1) (15), and c = 8.3908(3) Å, β = 109.209(3)° for compound **2**) are very close to these determined by single-crystal XRD, and the reliability factors (R_p and wR_p) are 0.0580 and 0.0878 for compound **1**, respectively, and 0.0558 and 0.0809 for compound **2**, respectively. These results provide further evidences for the purity of our materials.

Crystal structures

Compound **1** crystallizes in the polar space group $Cmc2_1$ (No. 36). Its structure is composed of isolated IO_3^- and $[Au(IO_3)_4]^-$ ions, which are separated by K^+ ions (Figures 3 a–c). The asymmetric unit of compound **1** contains one K, one Au, and four I atoms (Figure 3 a). The Au(1), I(1), I(2), and I(3) atoms sit on the mirror plane perpendicular to [100], whereas the K(1) and I(4) atoms occupy the general sites. All I atoms are three-coordinated in IO_3 trigonal-pyramidal geometry, and the Au(1) atom is located in an AuO_4 approximate square-planar geometry

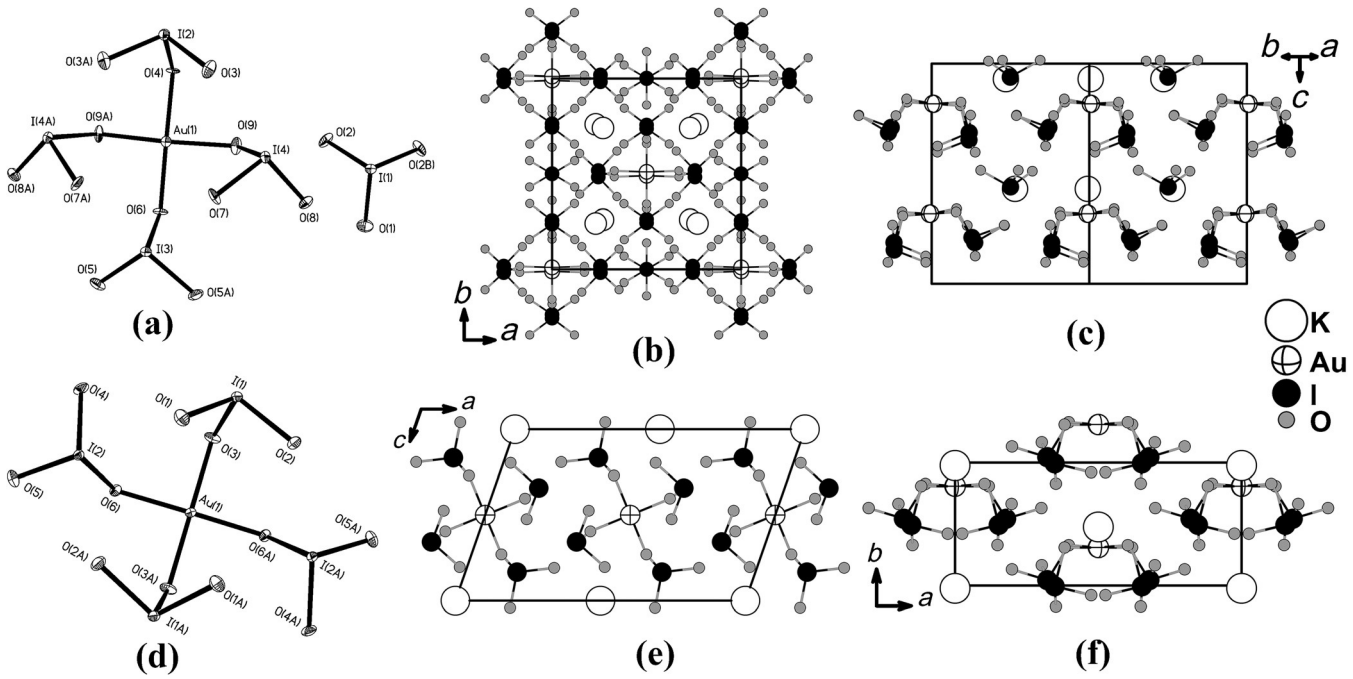

Figure 3. Structure view of $K_2Au(IO_3)_5$ and β-$KAu(IO_3)_4$: ORTEP representations of selected units for a) $K_2Au(IO_3)_5$ and d) β-$KAu(IO_3)_4$; view of the 3D structure along b) [001] and c) [110] for $K_2Au(IO_3)_5$, and along e) [010] and f) [001] for β-$KAu(IO_3)_4$. The thermal ellipsoids are drawn at the 30% probability level. Symmetry codes for the generated equivalent atoms for $K_2Au(IO_3)_5$: A = $-x$+1, y, z and B = $-x$, y, z and for β-$KAu(IO_3)_4$: A = $-x$+1, y, $-z$+1.

with four Au–O bond lengths ranging from 1.987(12) to 2.013(13) Å (Figure 3a). As the *trans*- and *cis*-O-Au-O angles of 173.9(8)/175.5(7) and 88.4(3)/91.4(4)° deviate slightly from the ideal values of 180 and 90°, respectively (Table S1 in the Supporting Information), the AuO_4 unit is distorted from the ideal D_{4h} symmetry. Each AuO_4 unit is corner-sharing with one $I(2)O_3$, one $I(3)O_3$, and two $I(4)O_3$ groups (all of them in a monodentate fashion), leading to the formation of a $[Au(IO_3)_4]^-$ group. All of the bridging O atoms (i.e., O(4), O(6), and O(9)) exhibit an obviously larger I–O bond length (1.900(17)/1.879(16)/1.908(13) Å) than those of the terminal I–O bonds (1.796(13)-1.828(12) Å), hence the terminal ones are double bonds, whereas the bridging ones are single bonds. The I-O-Au bond angles are 112.7(8), 120.1(8), and 118.1(7)°, which is close to those in other alkali metal gold iodates reported previously.[23,24b]

All four IO_3 units in a $[Au(IO_3)_4]^-$ group align at the same side of the AuO_4 plane, and the four I atoms virtually locate on a plane that is nearly parallel to the AuO_4 plane with a slightly dihedral angle of 1.48°. The average distance of the four I atoms from the AuO_4 plane is 1.553 Å. Such an asymmetric configuration of the $[Au(IO_3)_4]^-$ ion results in a high polarity. The $[Au(IO_3)_4]^-$ ion exhibits C_m symmetry with the mirror plane perpendicular to the *a* axis. Hence, the polarizations of the four IO_3 units add up along the *b* and *c* axes, giving great net polarizations for the $[Au(IO_3)_4]^-$ ion (Table S2 in the Supporting Information). Isolated $[I(1)O_3]^-$ ions also have C_m symmetry and possess net polarizations along the *b* and *c* axes. In the lattice, all $[Au(IO_3)_4]^-$ ions adopt an identical orientation with the AuO_4 planes being parallel to the *ab* plane. And all isolated $[I(1)O_3]^-$ ions are parallel with each other with their lone pair electrons aligning along the *c* axis (Figures 3b and c). Such a favorable arrangement of the $[Au(IO_3)_4]^-$ and $[I(1)O_3]^-$ ions results in the superposition of polarizations along the polar axis (i.e., the *c* axis), which arise the high polar nature of compound **1** (Table S2 in the Supporting Information).

Compound **2** crystallizes in the polar and chiral space group *C*2 (No. 5) and is isostructural with our previously reported $RbAu(IO_3)_4$ and α-$CsAu(IO_3)_4$.[24b] Its structure features isolated $[Au(IO_3)_4]^-$ ions separated by K^+ ions (Figures 3d–f). The asymmetric unit contains one K, one Au, and two I atoms (Figure 3d). Both the K(1) and Au(1) atoms are located on the two-fold rotation axis, whereas the I(1) and I(2) atoms occupy the general sites. The $Au(1)^{3+}$ ion connects with two $I(1)O_3$ and two $I(2)O_3$ units into a $[Au(IO_3)_4]^-$ group with the I-O-Au bond angles being 114.2(3)/120.3(3)° (Table S1 in the Supporting Information). Each IO_3 unit possesses two short I–O bonds (1.786(6)–1.799(6) Å) and one long I–O bond (1.891(7)–1.889(6) Å corresponding to the bridging oxygen atom). Within the $Au(1)O_4$ square-planar unit, the Au–O bond lengths are 1.973(5)/1.992(5) Å, and the *trans*- and *cis*-O-Au–O bond angles are 174.3(4)/180.0(4)° and 89.9(2)/90.1(2)°. The configuration of the $[Au(IO_3)_4]^-$ ion in compound **2** is similar to that in compound **1** with four IO_4 units aligning on the same side of the AuO_4 plane. The dihedral angle between the plane determined by the four I atoms and the AuO_4 plane is 1.85°, and the average distance of the four I atoms from the AuO_4 plane is 1.632 Å. Similar to that in compound **1**, the $[Au(IO_3)_4]^-$ ions in compound **2** are also highly polar (Table S2 in the Supporting Information). In the 3D lattice, the $[Au(IO_3)_4]^-$ ions are isolated from each other and aligned with identical orientation (Figures 3e and f), which yields an effective superposition of the polarizations.

Among the structures of the three polar potassium gold(III) iodates, compound **2** and α-$KAu(IO_3)_4$[23] exhibit quite similar structures and only contain isolated $[Au(IO_3)_4]^-$ ions, whereas compound **1** contains both $[Au(IO_3)_4]^-$ and "isolated" $[I(1)O_3]^-$ ions. For compound **2** and α-$KAu(IO_3)_4$, the arrangements of the $[Au(IO_3)_4]^-$ ions in the lattices are quite similar, but the local symmetry of the $[Au(IO_3)_4]^-$ ions is different. In α-$KAu(IO_3)_4$, despite the $Au(IO_3)_4$ unit is similar to that in compound **2** that four IO_3 units align at the same side of the AuO_4 plane, the four IO_3 have no symmetrical correlation and the $Au(IO_3)_4$ unit only possesses C_1 symmetry, whereas the $Au(IO_3)_4$ unit in compound **2** exhibits C_2 symmetry.

It is notable that the alkali-metal gold(III) iodate system exhibits great structural variability. Except compound **1**, all the other compounds possess the same formula, that is, $AAu(IO_3)_4$ (A = Na, K, Rb, and Cs) but crystallize in four different space groups: β-$NaAu(IO_3)_4$ in $P2_1/c$, α-$NaAu(IO_3)_4$ and α-$KAu(IO_3)_4$ in $P1$, compound **2**, $RbAu(IO_3)_4$ and α-$CsAu(IO_3)_4$ in $C2$, and β-$CsAu(IO_3)_4$ in $P\bar{1}$.[23,24b] For the centrosymmetric compounds, the four IO_3 within a $Au(IO_3)_4$ unit locate on both sides of the AuO_4 plane, and the $Au(IO_3)_4$ unit exhibits an ideal or an approximate C_{2h} local symmetry. For the non-centrosymmetric compounds, all the $Au(IO_3)_4$ units show great polarity as the four IO_4 units sit on the same side of the AuO_4 plane, and they show C_1 or C_2 local symmetry. Hence, the structural variability of the $AAu(IO_3)_4$ systems should be attributed to the large flexibility of the $Au(IO_3)_4$ building block.

Thermal stability studies

Thermogravimetric analysis (TGA) and differential scanning calorimetry (DSC) studies indicate that compounds **1** and **2** are both thermally stable up to 400 °C (Figure 4). The TGA and DSC curves for both compounds are quite similar. Both samples exhibit one strong endothermic peak (428 °C for compound **1** and 410 °C for compound **2**) on their DSC curves. The TGA curves show only one step of weight loss in the temperature ranges of 420–470 °C for compound **1** and 405–460 °C for compound **2**, corresponding to the endothermic peaks on the DSC curves. These features indicate that the samples are decomposing along further heating. The observed weight losses at 500 °C are 46.0% for compound **1** and 55.5% for compound **2**, which match well with their calculated values of 45.6% for compound **1** and 56.1% for compound **2**, corresponding to the releases of 1.5 I_2 and 4.5 O_2 molecules per formula unit for both compounds. Furthermore, the final residuals for the two compounds at 500 °C have been confirmed to be a mixture of KIO_3 and Au based on powder XRD studies (Figure S3 in the Supporting Information). Hence, the derived decomposition reactions are the ones given in Equations (1) and (2) for compounds **1** and **2**, respectively.

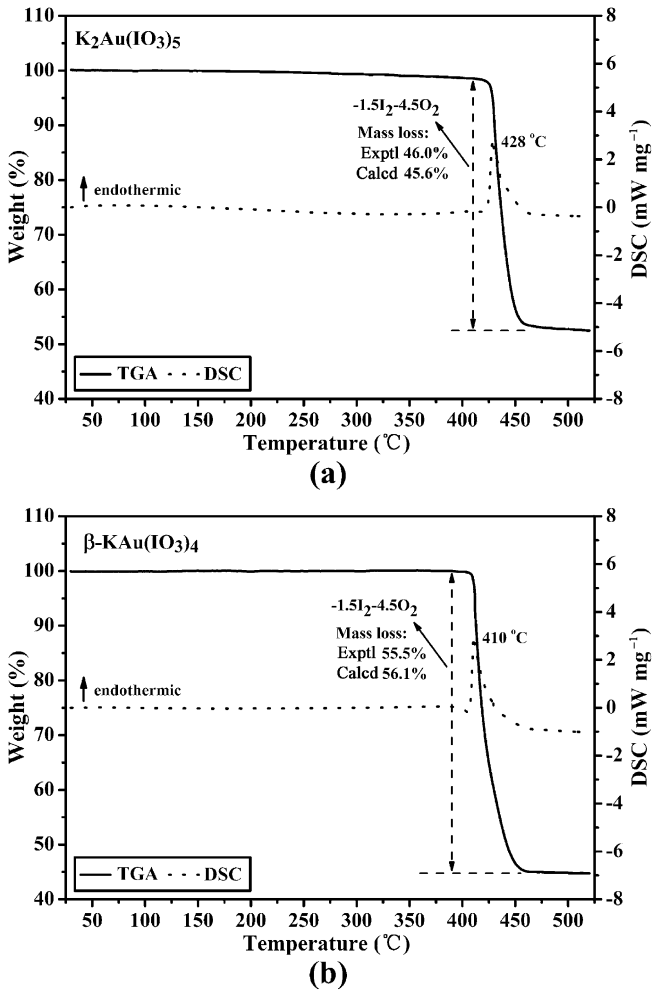

Figure 4. TGA and DSC curves for a) $K_2Au(IO_3)_5$ and b) β-$KAu(IO_3)_4$.

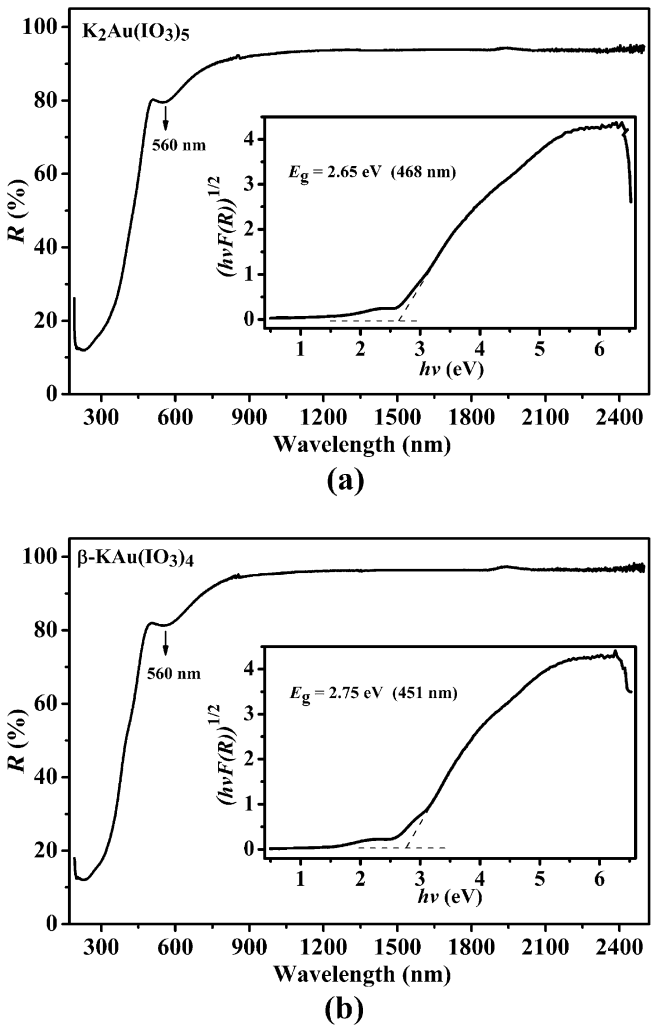

Figure 5. UV/Vis/NIR diffuse reflectance spectra of a) $K_2Au(IO_3)_5$ and b) β-$KAu(IO_3)_4$.

$$K_2Au(IO_3)_5 \xrightarrow{428\,^{\circ}C} 2\,KIO_3 + Au + 1.5\,I_2(\uparrow) + 4.5\,O_2(\uparrow) \quad (1)$$

$$\beta\text{-}KAu(IO_3)_4 \xrightarrow{410\,^{\circ}C} KIO_3 + Au + 1.5\,I_2(\uparrow) + 4.5\,O_2(\uparrow) \quad (2)$$

Vibrational spectra

The IR spectra of both compounds show the characteristic absorption bands of I–O stretching vibrations at $\tilde{\nu}=798$, 757, 739, 678, and 633 cm^{-1} for compound **1** and at $\tilde{\nu}=806$, 760, 741, 668, and 619 cm^{-1} for compound **2** (Figure S4 in the Supporting Information). The Au–O vibration bands appear at $\tilde{\nu}=$ 518 and 508 cm^{-1} for compound **1** and at $\tilde{\nu}=526$ and 502 cm^{-1} for compound **2**. These assignments are in agreement with those of other reported gold(III) iodates.[23,24b]

UV/Vis/NIR diffuse reflectance spectra

The UV/Vis/NIR diffuse reflectance spectra of both compounds **1** and **2** exhibit high reflectance in the region of $\lambda=800$–2500 nm (Figure 5), which indicates that the two compounds can serve as optical crystals in the NIR region. Below $\lambda=$ 800 nm, the reflectance spectra exhibit an absorption band with a maximum at about $\lambda=560$ nm for both compounds, which should be attributed to the metal-to-ligand charge-transfer (MLCT) processes within the AuO_4 structural units. And the following strong and sharp decrease of the reflectance below $\lambda=500$ nm is likely originating from the optical band-gap transition.

Furthermore, the band gaps were estimated by using the Tauc plot method (see the inset in Figure 5).[26] The absorption (α/S) data were calculated from the reflectance spectra by using the Kubelka–Munk function $F(R)=(1-R)^2/2R=\alpha/S$, and then the $[F(R)h\nu]^n$ values ($n=1/2$ or 2) were plotted against $h\nu$. Here the value of the exponent n donates the nature of the transition, that is, a direct transition for $n=2$ and an indirect transition for $n=1/2$, which can be determined based on the linearity of the Tauc plot above the band gap. By observing the plots with $n=2$ and 1/2, the $[F(R)h\nu]^{1/2}$ versus $h\nu$ plots show a larger linear range for both compounds **1** and **2**, which implies that both samples have an indirect band gap. Furthermore, through extrapolating the straightest line to the vertical axis in the $[F(R)h\nu]^{1/2}$ versus $h\nu$ plots, the indirect band gaps of compounds **1** and **2** were estimated to be 2.65 (468) and 2.75 eV (451 nm), respectively.

SHG properties

As compounds **1** and **2** exhibit high transmittance in the NIR range, the powder SHG effects of sieved crystals have been measured by using a 2.05 μm Q-switch laser. The plots of the SHG signals as a function of the particle size for compounds **1** and **2**, shown in Figure 6, indicate that both compounds are

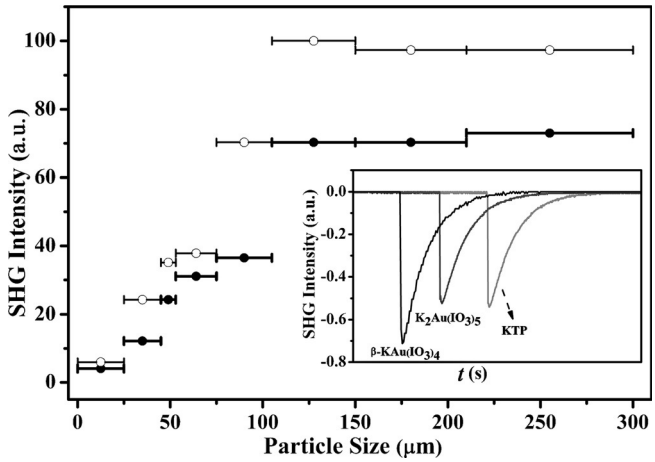

Figure 6. Curves of the measured SHG signals versus the particle sizes of $K_2Au(IO_3)_5$ (●) and β-$KAu(IO_3)_4$ (○) under laser radiation at $\lambda = 2.05$ μm. The oscilloscope traces of the SHG signals for the samples (150–210 μm) of $K_2Au(IO_3)_5$, β-$KAu(IO_3)_4$, and KTP are shown in the inset.

phase-matchable.[27] Furthermore, the SHG measurements of the sieved compounds **1** and **2** and KTP crystals all in the same particle range of 150–210 μm reveal that both compounds **1** and **2** exhibit strong SHG responses of approximately 1.0 and 1.3 times that of KTP, respectively (see the inset in Figure 6). Such excellent SHG responds imply that both compounds **1** and **2** are potential NIR NLO materials. The measured SHG response of compound **2** is comparable to that of reported $RbAu(IO_3)_4$ (1.33×KTP) and α-$CsAu(IO_3)_4$ (1.17×KTP). It is expected that the SHG effects should be mainly attributed to the $[Au(IO_3)_4]^-$ ions in the isostructural $AAu(IO_3)_4$ (A = K, Rb, and Cs) compounds and the contributions from the counter cations are negligible.

SHG measurements by using a $\lambda = 1064$ nm Q-switch laser have also been performed under the same conditions, and compounds **1** and **2** display large SHG responses of about 0.9 and 1.2 times that of KTP, respectively. Due to the absorption band with the maximum located at $\lambda = 560$ nm, the SHG signals at wavelength of 532 nm should be reduced by the absorption effect more or less. Hence, the intrinsic SHG conversion efficiency of a $\lambda = 1064$ nm laser is very hard to be assessed accurately.

According to the structure–property relationships, the excellent NLO property of compounds **1** and **2** should be attributed to their polar structure and the favorable arrangement of the AuO_4 plane and the IO_3 pyramidal unit in the lattices. As described above, all the $Au(IO_3)_4$ polar groups stack in an identical orientation in both compounds **1** and **2**. Furthermore, in compound **1**, the lone-pair electrons on the non-coordinated $I(1)O_3$ group are aligned in the same direction. These feature results in an effective superposition of the dipole moments of all the polar IO_3 units in the lattice along the polar axis for both compounds. To further assess the polar nature, calculations of the dipole moments for compounds **1** and **2** have been performed based on their geometric structure (Table S2 in the Supporting Information).[28] The local dipole moments of the IO_3 and AuO_4 units were calculated to be 13.008,13.211, 14.522, 15.012, and 1.357 D for compound **1**, 14.387, 15.713, and 0.814 D for compound **2**. Comparing with that of IO_3, the local dipole moments of the AuO_4 groups are negligible, which should be attributed to their nearly square-planar geometry. The net polarizations of an $Au(IO_3)_4$ group were calculated to be 28.573 D for compound **2** and 51.901 D for compound **1**. Finally, for both compounds **1** and **2**, only the components of the polarization along the polar axis add up in the unit cell, whereas the remaining components were cancelled out completely. The net dipole moment for the unit cells are 177.232 D for compound **1** (along the *c* axis) and 57.147 D for compound **2** (along the *b* axis). Taking into consideration the different unit-cell volumes, the dipole moments per unit volume are 0.114 and 0.099 D Å^{-3} for compounds **1** and **2**, respectively. Such large net dipole moments imply that the IO_3 polar units have adopted a favorable arrangement in the structures, which should be one main intrinsic factor for their strong SHG responses.

It is found that the calculated dipole moment per unit volume for compound **1** is slightly larger than that for compound **2**, whereas the measured SHG response of compound **1** is weaker than that of compound **2**. Such inverse tendency suggests that the non-polar AuO_4 plane unit may be another important part that also contributes to the SHG properties, which will be discussed in the following section.

Theoretical studies

Theoretical calculations have been performed to unveil the physical origins of the optical properties. The electronic band structures calculations give band gap of 1.92 eV for compound **1** and of 2.29 eV for compound **2**, showing the same magnitude trend with the experimental results, that is, compound **1** (2.65 eV) < compound **2** (2.75 eV). The deviations from the experimental values should be attributed to the limitation of the GGA-PBE function.[29] Hence, scissors of 0.73 and 0.46 eV for compounds **1** and **2**, respectively, have been added to shift up the conduction band levels for the following calculations and analyses. Due to the similarity of the chemical components and structural units in the title compounds, their band structures are very similar to each other (Figure S5 in the Supporting Information): for both compounds, the valence bands (VBs) are very flat, whereas the conduction bands (CBs) are relatively dispersed with several isolated bands in the bottommost level.

The partial density of states (PDOS) is a fundamental technique for assigning the band structure and studying the bonding interactions. As shown in Figure 7, the PDOS diagrams of

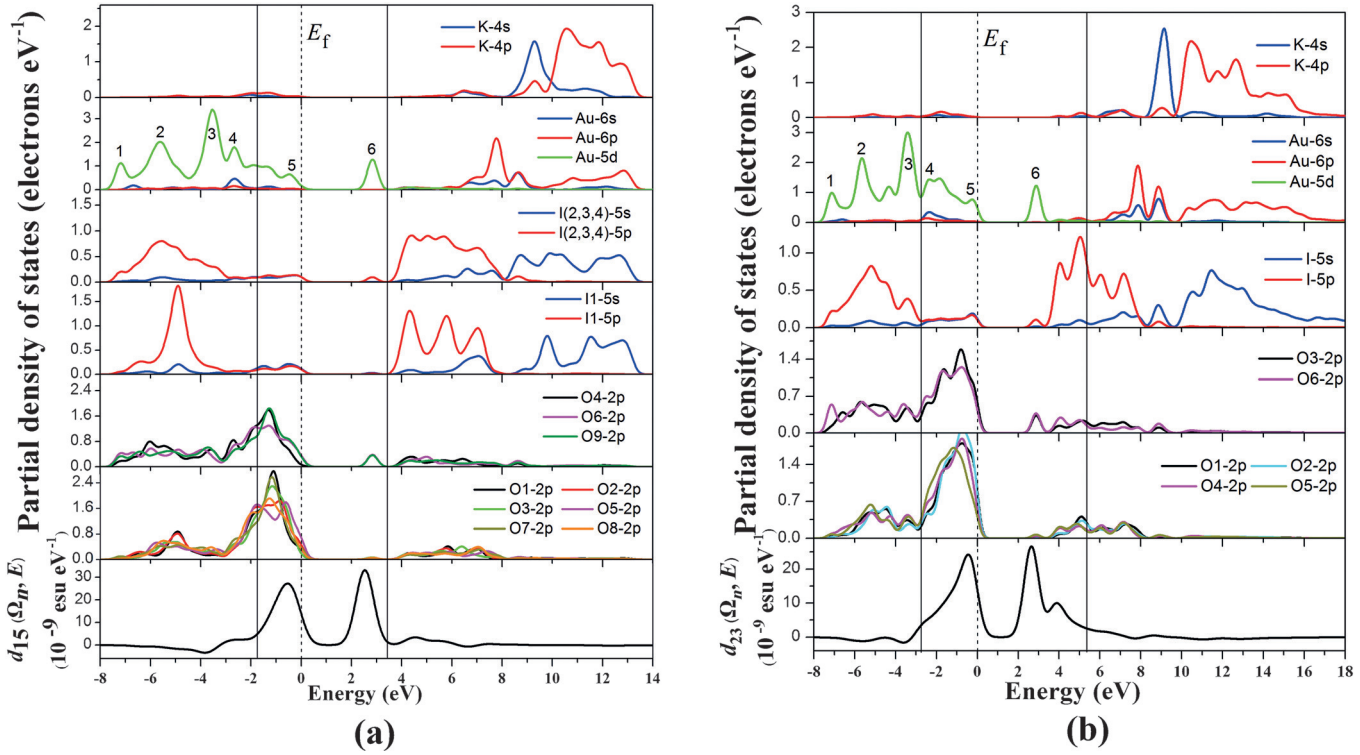

Figure 7. Partial density of states (the upper several panels) and the spectral decomposition of d_{in} (the bottommost panel) for a) $K_2Au(IO_3)_5$ and b) β-$KAu(IO_3)_4$.

the two compounds are quite similar, so we will take compound **1** as an example. In the VB and the CB, there is obvious overlap of the Au-5d and bridged O-2p, as well as of the I-5s5p and all O atoms, indicating the strong bonding interactions of the Au–O and I–O bonds. The s and p states of the K atoms only contribute to the bands far away from the Fermi level (K-3s3p: <-8.0 eV in the VB, K-4s: $\approx$9.3 eV in the CB, and K-4p: $\approx$9.7–13.3 eV in the CB). The VB top is dominated by non-bonding O-2p states, especially the 2p states of the terminal O atoms. As the bond valence sum of the terminal O atoms is much smaller than that of the bridging O atoms, the terminal O atoms have more O-2p non-bonding electrons which contribute to the larger PDOS peaks at the top of the VB. The bottommost CB mainly originates from the unoccupied $d_{x^2-y^2}$ orbital of Au, mixing with small amount of the 2p states of bridging O atom. So the band gap of compound **1** is determined by the Au and O atoms. According to the crystal field theory (CFT), the d orbitals of Au in a square-planar coordination geometry usually split into four energy levels: $d_{x^2-y^2} > d_{xy} > d_{z^2} > d_{xz} \approx d_{yz}$. Based on the calculated orbital graphs shown in Figure S6 in the Supporting Information, the PDOS peaks labeled by 2–5 in the Au panel are identified to belong to the d_{xy}, the mixture of d_{xz} and d_{yz}, d_{z^2}, and d_{xy}, respectively. The peak labeled by "1" is characterized by the strong σ bonding orbitals formed by the $d_{x^2-y^2}$ orbital of Au and O-2p, whereas the peak labeled with "6" in the bottommost CB is the antibonding state of the $d_{x^2-y^2}$ orbital of Au and O-2p.

The PDOS diagram of compound **2** is very similar to that of compound **1** (Figure 7); the slight difference is that the VB top of compound **2** comes not only from the nonbonding O-2p states, and also partly from Au-d_{xy}. The corresponding orbitals of these labeled Au-d peaks in the PDOS diagram of compound **2** are just the same as those of compound **1**, as shown in Figure S7 in the Supporting Information.

The SHG coefficients have been calculated for the title compounds based on the dielectric principle coordinate. For the monoclinic compound **2**, the calculated rotation angle between the crystallographic axes and the dielectric principle axes is 25.92°. Considering the restriction of Kleinman's symmetry, compounds **1** ($Cmc2_1$) and **2** ($C2$) have three (d_{15}, d_{24}, and d_{33}) and four (d_{14}, d_{16}, d_{22}, and d_{23}) independent SHG tensors, respectively. As listed in Table 2, the calculated largest tensors of the static SHG coefficients are $d_{15} = 3.35 \times 10^{-8}$ esu for compound **1** and $d_{23} = -3.76 \times 10^{-8}$ esu for compound **2**. Despite the calculated values are larger than the experimental results (1.0 and 1.3 times that of KTP for compounds **1** and **2**, respectively), the calculated results confirm the fact that both compounds **1** and **2** possess strong SHG effects.

Table 2. Calculated static SHG tensors for $K_2Au(IO_3)_5$ and β-$KAu(IO_3)_4$.

	$K_2Au(IO_3)_5$	β-$KAu(IO_3)_4$
calculated SHG coefficient tensors [$\times 10^{-8}$ esu]	$d_{15} = d_{31} = 3.35$ $d_{24} = d_{32} = 2.29$ $d_{33} = 3.19$	$d_{14} = d_{25} = d_{36} = 1.27$ $d_{16} = d_{21} = -3.54$ $d_{22} = -2.30$ $d_{23} = d_{34} = -3.76$

To investigate the origin of such strong SHG effects, we have performed the spectral decomposition of d_{15} for compound **1** and of d_{23} for compound **2**, which are plotted in the bottommost panels of Figure 7. For compound **1**, the most contributing regions are just the upper part of VB (−1.76 ~0 eV) and the bottommost CB (<3.44 eV) corresponding to the O-2p non-bonding states mixing with small amount of Au-d_{xy} states and the unoccupied antibonding states formed by Au-$d_{x^2-y^2}$ and bridged O-2p, respectively. Compared to compound **1**, compound **2** has a relatively broader contributed region in the CB, which extends to 5.35 eV. It suggests that except the Au–O antibonding states, the I-5p and other O-2p states also give some contributions to the SHG coefficient d_{23} in the CB of compound **2**.

To intuitively determine the SHG-contributing orbitals, SHG density analyses have been performed (Figure 8). For both compounds, the main contributions to the SHG coefficients in the VB come from the O-2p non-bonding states, especially the terminal O atoms which play a greater contribution to the DOS peaks in the VB top than the bridging O atoms. There is still a small contribution from Au-d_{xy} in the VB. The SHG contribution in the CB is mainly from empty antibonding states formed by Au-$d_{x^2-y^2}$ and bridging O-2p states, which confirmed the contribution of AuO_4 to the SHG effects. For compound **2**, except for the above-described contributions like compound **1**, the contributions of the I-5p orbitals in the CB cannot be ignored. The integral of the SHG density over the VB and the CB shows that the strong SHG efficiency originates mainly from the AuO_4 and IO_3 groups, and the contribution percentages of K^+ and the AuO_4 and IO_3 groups are 0.12, 21.2, and 75.0% for compound **1**, and 2.97, 20.8, and 73.3% for compound **2**, respectively. These results indicate that except for the IO_3 group, the AuO_4 group plays an important part in the SHG process. Hence, the strong SHG responses are originating from a synergistic effect of the AuO_4 and IO_3 units.

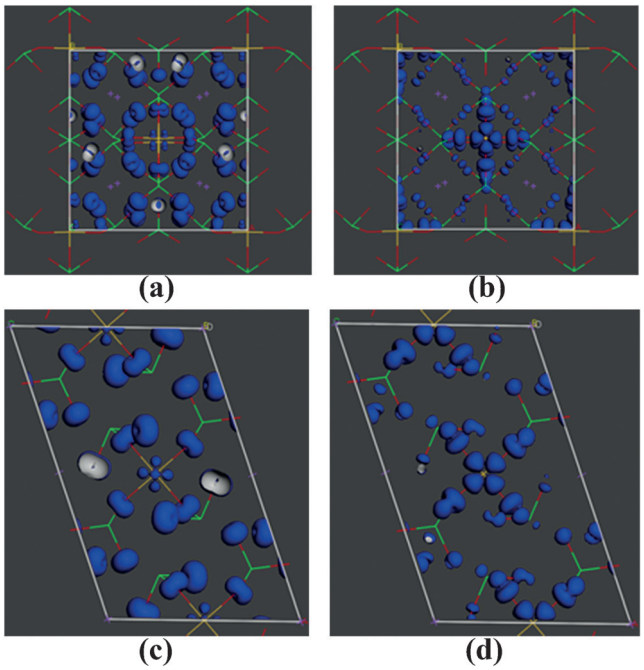

Figure 8. Calculated SHG density for $K_2Au(IO_3)_5$ [a) VB, b) CB] and β-$KAu(IO_3)_4$ [c) VB, d) CB].

Conclusion

Alkali–Au^{III}–iodate systems display a rich structure chemistry, and two new polar iodates, namely, $K_2Au(IO_3)_5$ (**1**, $Cmc2_1$) and β-$KAu(IO_3)_4$ (**2**, $C2$), have been prepared by using analogous synthesis procedures with the same starting materials. Compound **1** contains both isolated IO_3^- and $[Au(IO_3)_4]^-$ ions, whereas compound **2** only contains $[Au(IO_3)_4]^-$ ions. These isolated anions are separated by K^+ ions in both compounds. Both compounds **1** and **2** exhibit strong SHG responses (1.0 and 1.3 times that of KTP, respectively) based on powder SHG measurements by using $\lambda = 2.05$ μm laser radiation, high transmittance in the spectral region of $\lambda = 800$–2500 nm, and high thermal stability up to 400 °C. Such intriguing overall properties are indicative of their potential applications as near-infrared NLO crystals. Furthermore, theoretical calculations based on DFT methods suggest that their strong SHG responses originate from a synergistic effect of the AuO_4 and IO_3 units. Hence, introduction AuO_4 units into metal iodates is an effective strategy for the design and synthesis of new state-of-the-art NLO materials.

Experimental Section

Characterization: Room temperature powder XRD patterns were recorded on a Rigaku MiniFlex II diffractometer with monochromated $Cu_{K\alpha}$ radiation ($\lambda = 1.540598$ Å). The data were collected with a step size of 0.02° over the 2θ range of 5–85°. Microprobe elemental analyses were carried out on a field emission scanning electron microscope (FESEM, JSM6700F) equipped with an energy-dispersive X-ray spectroscope (EDS, Oxford INCA). Thermogravimetric analyses (TGA) and differential scanning calorimetry (DSC) were performed simultaneously on a NETZSCH STA 449F3 instrument. The ground crystals loaded in an alumina pan were heated under a flowing N_2 atmosphere with a heating rate of 10 °C min^{-1}. Infrared (IR) spectra were recorded on a Nicolet AVATAR 370 FTIR spectrophotometer in the range of $\tilde{\nu} = 4000$–400 cm^{-1}. Crystals were ground and then dispersed in KBr pellets. The UV/Vis/NIR optical diffuse reflectance spectra were recorded at room temperature on a Perkin–Elmer Lambda 950 Spectrophotometer with a wavelength range of $\lambda = 190$–2500 nm. A $BaSO_4$ plate was used as a standard (100% reflectance).

Powder frequency-doubling effects for the two title compounds were assessed based on the modified Kurtz and Perry's method.[27] Radiations of $\lambda = 1064$ nm and a $\lambda = 2.05$ μm generated by a Q-switched Nd:YAG solid-state laser were used as the fundamental frequency light, respectively. Crystals of compounds **1** and **2** were ground and sieved into a series of particle size ranges (0–25, 25–45, 45–53, 53–75, 75–105, 105–150, 150–210, and 210–300 μm), and then they were pressed into the sample loading area with thickness of 1.2 mm and a diameter of 8 mm. Sieved KTP crystals with the corresponding size ranges were used as references.

Syntheses: Both compounds **1** and **2** were synthesized by using a versatile hydrothermal method with the same starting materials of KIO_3 (≥99.8%, Sinopharm), $Au(OH)_3$ (≥79.0%, Alfa Aesar), and I_2O_5 (≥99.0%, Sinopharm). The optimal-loaded compositions were KIO_3 (107.0 mg, 0.5 mmol), $Au(OH)_3$ (6.2 mg, 0.025 mmol), I_2O_5 (2002.9 mg, 6.0 mmol), and H_2O (3 mL) for compound **1**, and KIO_3 (107.0 mg, 0.5 mmol), $Au(OH)_3$ (24.8 mg, 0.10 mmol), I_2O_5 (1335.2 mg, 4.0 mmol), and H_2O (3 mL) for compound **2**. The mixture was sealed in a 15 mL Teflon-lined stainless steel autocalve and heated at 235 °C for 30 (for compound **1**) or 72 h (for compound **2**), followed by slow cooling to 35 °C with a rate of 2 °C h^{-1}. Yellow prism-shaped crystals of compound **1** (Figure 1a) and yellow granular crystals of compound **2** (Figure 1b) were obtained in yields of about 63 and 65% (based on $Au(OH)_3$), for compounds **1** and **2**, respectively, with little amount of Au powder. Clear away the impurity, pure phases crystals of compounds **1** and **2** were obtained, which were confirmed by powder XRD studies (Figure 2).

Single-crystal structures determination: Transparent single crystals of compounds **1** and **2** with dimensions of 0.16×0.13×0.09 mm^3 and 0.14×0.12×0.08 mm^3, respectively, were selected for single-crystal XRD. The data collections were performed on an Agilent Technologies SuperNova Dual Wavelength CCD diffractometer employing $Mo_{K\alpha}$ radiation (λ = 0.71073 Å) at room temperature. The program CrysAlisPro was used to perform data reduction, and the multi-scan method was applied for absorption correction.[30] Both structures were solved by using direct methods and refined by full-matrix least-squares fitting on F^2 by using SHELX-97.[31] Racemic twinning was confirmed according to the TwinRotMat calculation based on the data of compound **1**, and instructions TWIN 0 -1 0 -1 0 0 0 0 0 1 and BASF 0.25556 were applied for structure refinement.[32] For compound **1**, no twinning was found and the refined Flack parameters was −0.033(6), which is indicative of correctness of its absolute structures.[33] The space groups for both structures were finally confirmed by using PLATON.[34] The crystallographic data are summarized in Table 1, and selected bond lengths and angles are listed in Table S1 in the Supporting Information. Further details of the crystal structure investigation(s) can be obtained from the Fachinformationszentrum Karlsruhe, 76344 Eggenstein-Leopoldshafen, Germany (fax: (+49) 7247-808-666; e-mail: crysdata@fiz-karlsruhe.de, http://www.fiz-karlsruhe.de/request_for_deposited_data.html) on quoting the depository numbers CSD-430304 and 430305 for compounds **1** and **2**, respectively.

Computational methods: Calculations of the electronic structure and the NLO properties for the two title compounds were performed by using CASTEP based on density function theory (DFT).[35,36] A norm-conserving pseudopotential was used to treat the electron–core interactions, and the GGA-PBE exchange-correlation function was employed for band structures and density of states (DOS) calculations.[37,38] The following orbital electrons were treated as valence electrons: K-$3s^2 3p^6 4s^1$, Au-$5d^{10} 6p^1$, I-$5s^2 5p^5$, and O-$2s^2 2p^4$. The numbers of plane waves included in the basis sets were determined by a cutoff energy of 750 eV for both compounds, and Monkhorst–Pack *k*-point sampling of 3×3×2 and 2×5×3 was adopted for compounds **1** and **2**, respectively.

Calculations of the SHG susceptibility were performed according to the static formula developed by Rashkeev et al. and Chen et al. based on a length-gauge formalism within the independent-particle approximation.[39–41] To ensure the convergence of the SHG coefficients, 240 and 616 empty bands were used for the calculations for compounds **1** and **2**, respectively.

Acknowledgements

Financial support from the National Natural Science Foundation of China (Nos. 21231006, 21203197, and 21401194) and the Natural Science Foundation of Fujian Province (Nos. 2015J05045 and 2013J01065) is gratefully acknowledged.

Keywords: iodine · polar material · second-harmonic generation · single-crystal structures · synergistic effects

[1] a) C. H. Hu, J. G. Mao, *Coord. Chem. Rev.* **2015**, *288*, 1–17; b) C. F. Sun, B. P. Yang, J. G. Mao, *Sci. China Chem.* **2011**, *54*, 911–922.
[2] M. S. Wickleder, *Chem. Rev.* **2002**, *102*, 2011–2087.
[3] W. Wang, B. Huang, X. Ma, Z. Wang, X, Qin, X. Zhang, Y. Dai, M. Whangbo, *Chem. Eur. J.* **2013**, *19*, 14777–14780.
[4] M. B. Taouti, Y. Suffren, O. Leynaud, D. Benbertal, A. Brenier, I. Gautier-Luneau, *Inorg. Chem.* **2015**, *54*, 3608–3618.
[5] H. W. Huang, Y. He, R. He, Z. S. Lin, Y. H. Zhang, S. C. Wang, *Inorg. Chem.* **2014**, *53*, 8114–8119.
[6] S. D. Nguyen, J. Yeon, S. H. Kim, P. S. Halasyamani, *J. Am. Chem. Soc.* **2011**, *133*, 12422–12425.
[7] a) G. Nath, S. Haussühl, *Phys. Lett. A* **1969**, *29*, 91–92; b) J. Jerphagnon, *Appl. Phys. Lett.* **1970**, *16*, 298–299.
[8] S. K. Kurtz, T. T. Perry, J. G. Bergman, *Appl. Phys. Lett.* **1968**, *12*, 186–188.
[9] N. Ye, Q. X. Chen, B. C. Wu, C. T. Chen, *J. Appl. Phys.* **1998**, *84*, 555–558.
[10] A. Fischer, *Acta Crystallogr. Sect. E* **2005**, *61*, i278–i279.
[11] K. M. Ok, P. S. Halasyamani, *Angew. Chem. Int. Ed.* **2004**, *43*, 5489–5491; *Angew. Chem.* **2004**, *116*, 5605–5607.
[12] D. Phanon, I. Gautier-Luneau, *Angew. Chem. Int. Ed.* **2007**, *46*, 8488–8491; *Angew. Chem.* **2007**, *119*, 8640–8643.
[13] a) K. M. Ok, P. S. Halasyamani, *Inorg. Chem.* **2005**, *44*, 9353–9359; b) I. Gautier-Luneau, Y. Suffren, H. Jamet, J. Pilmé, *Z. Anorg. Allg. Chem.* **2010**, *636*, 1368–1379; c) X. Xu, B. P. Yang, C. Huang, J. G. Mao, *Inorg. Chem.* **2014**, *53*, 1756–1763.
[14] X. Xu, C. L. Hu, B. X. Li, B. P. Yang, J. G. Mao, *Chem. Mater.* **2014**, *26*, 3219–3230.
[15] a) R. E. Sykora, K. M. Ok, P. S. Halasyamani, T. E. Albrecht-Schmitt, *J. Am. Chem. Soc.* **2002**, *124*, 1951–1957; b) R. E. Sykora, K. M. Ok, P. S. Halasyamani, D. M. Wells, T. E. Albrecht-Schmitt, *Chem. Mater.* **2002**, *14*, 2741–2749; c) T. C. Shehee, R. E. Sykora, K. M. Ok, P. S. Halasyamani, T. E. Albrecht-Schmitt, *Inorg. Chem.* **2003**, *42*, 457–462.
[16] a) H. Y. Chang, S. H. Kim, P. S. Halasyamani, K. M. Ok, *J. Am. Chem. Soc.* **2009**, *131*, 2426–2427; b) H. Y. Chang, S. H. Kim, K. M. Ok, P. S. Halasyamani, *J. Am. Chem. Soc.* **2009**, *131*, 6865–6873.
[17] Y. Suffren, I. Gautier-Luneau, *Eur. J. Inorg. Chem.* **2012**, 4264–4267.
[18] a) C. F. Sun, C. L. Hu, X. Xu, J. B. Ling, T. Hu, F. Kong, X. F. Long, J. G. Mao, *J. Am. Chem. Soc.* **2009**, *131*, 9486–9487; b) C. F. Sun, C. L. Hu, X. Xu, B. P. Yang, J. G. Mao, *J. Am. Chem. Soc.* **2011**, *133*, 5561–5572; c) B. P. Yang, C. L. Hu, X. Xu, C. F. Sun, J. H. Zhang, J. G. Mao, *Chem. Mater.* **2010**, *22*, 1545–1550; d) B. P. Yang, C. L. Hu, X. Xu, C. Huang, J. G. Mao, *Inorg. Chem.* **2013**, *52*, 5378–5384.
[19] C. F. Sun, C. L. Hu, J. G. Mao, *Chem. Commun.* **2012**, *48*, 4220–4222.
[20] X. A. Chen, X. A. Chang, H. G. Zang, Q. Wang, W. Q. Xiao, *J. Alloys Compd.* **2005**, *396*, 255–259.
[21] Y. H. Kim, T. T. Tran, P. S. Halasyamani, K. M. Ok, *Inorg. Chem. Front.* **2015**, *2*, 361–368.
[22] a) P. S. Halasyamani, *Chem. Mater.* **2004**, *16*, 3586–3592; b) K. M. Ok, P. S. Halasyamani, *Chem. Mater.* **2006**, *18*, 3176–3183.
[23] J. Ling, T. E. Albrecht-Schmitt, *Eur. J. Inorg. Chem.* **2007**, 652–655.
[24] a) C. F. Sun, C. L. Hu, X. Xu, J. G. Mao, *Inorg. Chem.* **2010**, *49*, 9581–9589; b) C. Huang, C. L. Hu, X. Xu, B. P. Yang, J. G. Mao, *Inorg. Chem.* **2013**, *52*, 11551–11562.
[25] B. H. Toby, *J. Appl. Crystallogr.* **2001**. *34*, 210–213.
[26] a) J. Tauc, R. Grigorovici, A. Vancu, *Phys. Stat. Sol.* **1966**, *15*, 627–637; b) J. Tauc, *Mater. Res. Bull.* **1968**, *3*, 37–46.
[27] S. K. Kurtz, T. T. Perry, *J. Appl. Phys.* **1968**, *39*, 3798–3813.

[28] a) J. Galy, G. Meunier, S. Andersson, A. Åström, *J. Solid State Chem.* **1975**, *13*, 142 – 159; b) H. K. Izumi, J. E. Kirsch, C. L. Stern, *Inorg. Chem.* **2005**, *44*, 884 – 895.
[29] a) R. W. Godby, M. Schlüther, L. J. Sham, *Phys. Rev. B* **1987**, *36*, 6497 – 6500; b) C. M. I. Okoye, *J. Phys. Condens. Matter* **2003**, *15*, 5945 – 5958.
[30] R. H. Blessing, *Acta Crystallogr. Sect. A* **1995**, *51*, 33 – 38.
[31] SHELXTL Version 5.1, G. M. Sheldrick, Crystallographic Software Package, Bruker-AXS, Madison, WI, **1998**.
[32] H. D. Flack, *J. Appl. Cryst. Sect. A* **1987**, *43*, 564 – 568.
[33] a) H. D. Flack, *Acta Crystallogr. Sect. A* **1983**, *39*, 876 – 881; b) H. D. Flack, G. Bernardinelli, *Chirality* **2008**, *20*, 681 – 690.
[34] a) A. L. Spek, *Acta Crystallogr. Sect. D* **2009**, *65*, 148 – 155; b) A. L. Spek, *J. Appl. Crystallogr.* **2003**, *36*, 7 – 13.
[35] M. D. Segall, P. J. D. Lindan, M. J. Probert, C. J. Pickard, P. J. Hasnip, S. J. Clark, M. C. Payne, *J. Phys. Condens. Matter* **2002**, *14*, 2717 – 2744.
[36] V. Milman, B. Winkler, J. A. White, C. J. Pickard, M. C. Payne, E. V. Akhmatskaya, R. H. Nobes, *Int. J. Quantum Chem.* **2000**, *77*, 895 – 910.
[37] J. P. Perdew, K. Burke, M. Ernzerhof, *Phys. Rev. Lett.* **1996**, *77*, 3865 – 3868.
[38] J. S. Lin, A. Qteish, M. C. Payne, V. Heine, *Phys. Rev. B* **1993**, *47*, 4174 – 4180.
[39] C. Aversa, J. E. Sipe, *Phys. Rev. B* **1995**, *52*, 14636 – 14645.
[40] S. N. Rashkeev, W. R. L. Lambrecht, B. Segall, *Phys. Rev. B* **1998**, *57*, 3905 – 3919.
[41] J. Li, M. H. Lee, Z. P. Liu, C. T. Chen, C. J. Pickard, *Phys. Rev. B* **1999**, *60*, 13 380 – 13 389.

Received: October 13, 2015
Published online on January 7, 2016